

Article

Understanding the Fatigue Notch Sensitivity of High-Strength Steels through Fracture Toughness

Sergi Parareda ^{1,2,*} , David Frómeta ¹ , Daniel Casellas ^{1,3} , Henrik Sieurin ⁴ and Antonio Mateo ² 

¹ Eurecat, Centre Tecnològic de Catalunya, Unit of Metallic and Ceramic Materials, 08243 Manresa, Spain; david.frometa@eurecat.org (D.F.); daniel.casellas@eurecat.org (D.C.)

² CIEFMA—Department of Materials Science and Engineering, EEBE, Universitat Politècnica de Catalunya, BarcelonaTech, 08019 Barcelona, Spain; antonio.manuel.mateo@upc.edu

³ Division of Solid Mechanics, Luleå University of Technology, 971 87 Luleå, Sweden

⁴ Scania AB, Materials Technology Department, 151 87 Södertälje, Sweden; henrik.sieurin@scania.com

* Correspondence: sergi.parareda@eurecat.org

Abstract: This study presents an innovative approach for selecting high-strength materials for fatigue dimensioning parts, considering both fracture toughness and fatigue performance. Warm and hot forming processes enable the construction of high-strength parts above 1000 MPa with complex geometries, making them suitable for lightweight chassis in automotive and freight applications. This research reveals that high-strength steels can experience up to a 40% reduction in fatigue performance due to manufacturing defects introduced during punching and trimming. Fracture toughness has been proposed as a good indicator of notch sensitivity, with a strong correlation of 0.83 between fracture toughness and fatigue notch sensitivity. Therefore, by combining fracture toughness measurements and fatigue resistance obtained through the rapid fatigue test, it becomes possible to quickly identify the most fatigue-resistant materials to deal with defects. Among the nine materials analysed, warm-formed steels show promising characteristics for lightweight chassis construction, with high fatigue resistance and fracture toughness exceeding the proposed fracture threshold of 250 kJ/m².

Keywords: fracture toughness; fatigue; chassis parts; high strength steel; sheared edge; warm forming steels



Citation: Parareda, S.; Frómeta, D.; Casellas, D.; Sieurin, H.; Mateo, A. Understanding the Fatigue Notch Sensitivity of High-Strength Steels through Fracture Toughness. *Metals* **2023**, *13*, 1117. <https://doi.org/10.3390/met13061117>

Academic Editor: Roumen Petrov

Received: 11 May 2023

Revised: 5 June 2023

Accepted: 10 June 2023

Published: 14 June 2023



Copyright: © 2023 by the authors. Licensee MDPI, Basel, Switzerland. This article is an open access article distributed under the terms and conditions of the Creative Commons Attribution (CC BY) license (<https://creativecommons.org/licenses/by/4.0/>).

1. Introduction

Many metallic structures experience cyclic loading during their lifetime, which can potentially compromise their integrity, even if they are loaded below the yield strength of the material. A prime example of such structures are automotive chassis parts, which are exposed to high cyclic stresses during vehicle operation [1–5]. Despite the high quality required for these parts, the need for greater transport efficiency and lightweight construction is driving innovation in the truck market [6,7]. Currently, chassis parts are typically manufactured using mild- and high-strength low alloy (HSLA) steel sheets, which exhibit good mechanical properties but are not sufficient to achieve significant weight reductions. However, the industry can adopt the lightweighting strategies developed for the body in white components of passenger vehicles by using high-strength steels [8]. Sheet-forming processes such as press-hardening or warm-forming can be employed to form high-strength steels, resulting in even lighter parts with complex shapes which can withstand higher loads.

Fatigue is a phenomenon in which plastic deformation accumulates due to cyclic loading, resulting in crack initiation, propagation, and eventual fracture of a component. This localised plastic deformation occurs at the most stressed site, which can be promoted by a poor component design or surface defects introduced during part manufacturing. In chassis parts, these surface irregularities are often introduced in the sheet shearing process (trimming, punching, etc.). It has been shown that the sheared edge morphology depends on various factors, including the material, punch geometry, shearing clearance,

and tool wear [9,10]. Some strategies have been developed to overcome such problems. Angled punches reduce the shearing forces but also the quality of the edge [11]. The angle between the punch and the sheet induces lateral forces in the punch that varies the cutting clearance [12]. Using worn tools or a high clearance leads to excessive plastic deformation, fracture angle, and burr, while sharp tools and small clearances may produce undesired burnish zones and secondary cracks [13]. Moreover, the defects on the shear edge may compromise the sheet's formability if the next forming steps involve bending or stretching operations, resulting in edge cracks. This phenomenon is well known in sheet forming of high-strength materials; furthermore, it is named edge cracking. Frómeta et al. [14] showed that fracture toughness is a valuable parameter to rank the edge cracking resistance of high-strength steels and to evaluate the resistance to crack propagation. It has been shown that high-toughness steels have higher resistance to edge cracking [15]. Similarly, the shape of the sheared edge affects the fatigue resistance of the components [16]. Several authors have shown that the defects in the sheared edge govern fatigue resistance as they act as stress raisers and crack initiation points [17–20]. Multiple solutions have been proposed to improve the fatigue resistance of the sheared edge, such as the two-stage shearing process. The technique leaves a cutting offset cut in a consecutive shearing operation resulting in a less damaged edge and better surface quality. The process highly improves the formability and fatigue resistance of the sheared material [21]. Another technique relies on introducing compressive residual stresses to the sheared edge through shot-peening and coining processes [22–24]. Although the fatigue results are improved, fatigue strength is still reduced after shearing the material, which is more relevant in materials with higher yield strength. In fact, the edge-cutting method is especially relevant in high-strength steels where the defects could decrease the fatigue resistance by more than 30–40% [25–27].

Numerous theories and methods have been developed to analyse the fatigue notch effect by using the concept of stress gradient [28,29]. Nonetheless, obtaining the necessary data, such as fatigue threshold and fatigue limit, to input into these models remains time-consuming. Although thermographic technologies appear to facilitate the rapid determination of the fatigue limit for regular specimen shapes or notched geometries [30,31], it is important to note that the thermal signal may be influenced by external sources, which could compromise the analysis [32]. This limitation can be overcome by employing the rapid testing method based on strain measurements [33]. In this work, coupling this method with fracture toughness as an experimental tool is proposed to rapidly assess the impact of notches on fatigue of high-strength steels. The aim is to expedite the material selection process for fatigue applications.

2. Materials and Methods

2.1. Materials

The nine investigated materials cover the primary microstructures of cold and hot-rolled high-strength steel sheets, from ferrite–pearlite steel to a fully martensitic microstructure. The HSLA S500MC steel exhibits a ferritic–pearlitic microstructure such as the high-drawing quality mild steel MS300 but with a very fine dispersion of alloy carbides. The ferritic–bainitic matrix with martensite and austenite islands of the hot rolled complex phase (CP) steel HR800CP shows similar mechanical properties to the ferritic–bainitic S700MC. A good balance between formability and strength is achieved by the dual-phase steels combining a soft ferrite matrix with martensite islands, leading to excellent strain hardening and elongation at failure. Cold forming of DP1000 allows the production of parts with greater resistance than the HSLA steels; however, the high elevated stamping loads and the associated high springback hamper their application to form complex shape parts. One alternative is the warm forming process, a similar strategy to the well-known hot forming process but at lower forming temperatures and without reaching the austenitizing temperature (A_{c3}). Both solutions are based on heating the material to increase its formability. In the hot forming, the material is heated above A_{c3} , hot-formed and die-quenched. This is the case of the studied fully martensitic press-hardened steel 22MnB5 (Figure 1d).

Warm forming consists in heating the blank around 600 °C for 4 min, warm forming, and air-cooling. The technology has the benefit of being able to form lighter and more complex components made of high-strength hot-rolled steel grades. A further advantage of this process is that no sheet coatings are required. Cracks in the coating produced by thermal mismatch affect the fatigue behaviour as these cracks act as fatigue initiation points as observed in press-hardening B steels [34]. In the as-received condition, the WL750 grade presents a bainitic microstructure (Figure 1a). After warm forming, the alloying elements form fine dispersed alloy carbides in the bainitic matrix. The WL980 and WL1150 grades show a fully martensitic microstructure in the as-received condition, which form tempered martensite after the heat treatment as shown in Figure 1b,c, decreasing the yield strength and ultimate strength. The rough chemical composition of the investigated materials is given in Table 1.

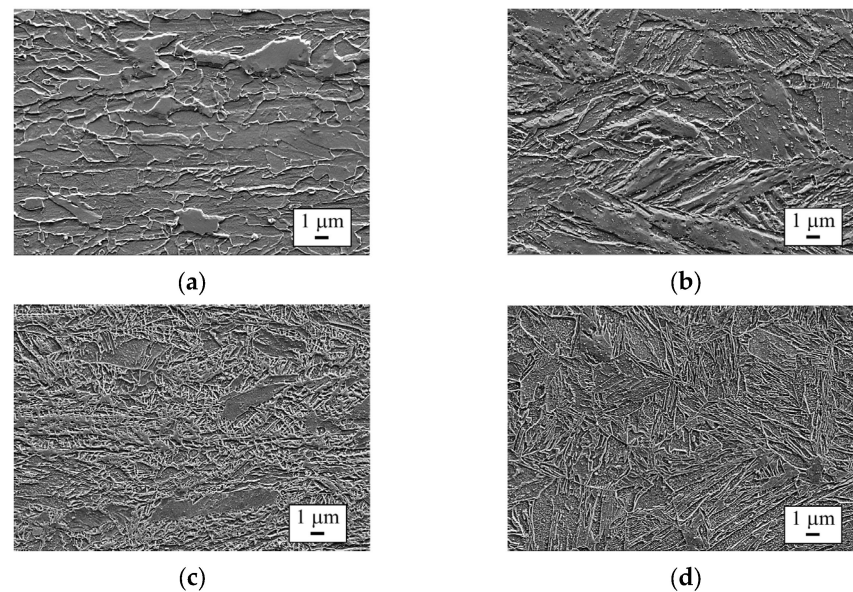


Figure 1. Microstructures of the studied warm and hot forming materials (a) WL750, (b) WL980 (c) WL1150, and (d) 22MnB5 in their final state.

Table 1. Chemical composition of the investigated materials in weight percentage; the balance is Fe.

Steel Grade	C	Si	Mn	Cr	Al
MS300	0.09	0.01	0.3	0.02	0.03
S500MC	0.16	0.5	1.2	-	-
WL750	0.06	-	1.9	-	-
HR800CP	0.18	1.0	2.2	-	-
S700MC	0.12	0.5	1.6	-	-
WL980	0.09	-	1.6	~1	-
DP1000	0.17	0.48	1.56	0.05	0.05
WL1150	0.18	-	-	-	-
22MnB5	0.25	0.29	1.23	0.2	0.04

Conventional axial tensile tests were performed for the different microstructures in a universal testing machine according to ISO 6892 standard. The tensile specimens were machined transverse to the rolling direction. The results are reported in Table 2, with the microstructure corresponding to each steel grade.

Table 2. Material thickness (t), tensile parameters in terms of yield strength (σ_{YS}), ultimate tensile strength (σ_{UTS}) and elongation at fracture (A_{80} , gauge length 80 mm). Microstructural phases: ferrite (F), pearlite (P), bainite (B), martensite (M), and austenite (A).

Steel Grade	t [mm]	σ_{YS} [MPa]	σ_{UTS} [MPa]	A_{80} [%]	Microstructure
MS300	1.5	217	299	28	F matrix-P islands
S500MC	6	641	651	27	F matrix-P islands
WL750	7	806	807	17	B
HR800CP	5	819	881	18	F/B matrix-M/A islands
S700MC	6	825	935	19	F-B
WL980	7	1051	1054	11	Tempered M
DP1000	2	798	1059	6	F-M
WL1150	7	1201	1203	9	Tempered M
22MnB5	1.8	1346	1543	6	M

2.2. Fatigue Tests

The fatigue strength was evaluated in terms of fatigue strength (σ_f) at $2 \cdot 10^6$ cycles, which is defined as the fatigue limit for the high cycle fatigue (HCF) regime [35] and is commonly used in the automotive industry [36]. It was determined through the conventional testing method following the ISO 1099 recommendations. At least 15 specimens were used for each material in the staircase tests according to Dixon–Mood method [37]. Moreover, the fatigue resistance of the warm-forming materials was determined by testing 3 specimens using the *stiffness method* described in the reference [38]. The stepwise method consisted in increasing the maximum stress (σ_{max}) after a loading block of 6000 cycles. The stress is increased by 25 MPa between each block up to the fracture of the specimen, as schematically described in Figure 2. The test starts with a σ_{max} of 50 MPa, which is below the expected σ_f . The damage introduced during the test was monitored through the total strain range measurements ($\Delta\epsilon_i$) performed at the beginning of the test when the material was non-damaged and after each fatigue block. $\Delta\epsilon_i$ was measured at a nominal elastic stress of $\sigma_{YS}/2$ using a loading–unloading rate of 5 MPa/s. The strain measurements were carried out using a 3D Digital Image Correlation (DIC) GOM Aramis SRX, Class 0.5 according to ISO 9513. The system was equipped with an external blue LED light to illuminate the painted specimen and avoid the effect of the ambient light of the laboratory. The exposure time was less than 5 ms, and the frame rate was 25 Hz. The cameras mounted onto the testing machine were calibrated before the test session using a coded panel of 150 mm by 120 mm. The facet size used was 11×11 pixels, and the initial length (L_0) of the virtual extensometer placed on the fatigue specimen was 20 mm. Once the specimen was broken, the strain progress rate ($d\Delta\epsilon_i/dN$) was evaluated to identify the three regimes linked to the fatigue damage: (i) incipient damage, (ii) microcrack formation, and (iii) macrocrack propagation. The regimes (i) and (ii) were used to quantify the fatigue damage (D) according to:

$$D = \frac{\Delta\epsilon_p - \Delta\epsilon_{p0}}{\Delta\epsilon_{pf} - \Delta\epsilon_{p0}} \quad (1)$$

where $\Delta\epsilon_{p0}$ and $\Delta\epsilon_{pf}$ are the initial and final inelastic strains, respectively, and $\Delta\epsilon_p$ is the inelastic strain after each fatigue block. As shown in Figure 2c, the σ_f was determined by the interception of the fitting line to the x -axis in the plot of the inelastic strains ($\Delta\epsilon_p$) against the maximum stress (σ_{max}). The selected points for the fitting line are the points that describe the microcrack propagation. In this method, only three specimens were required to determine the fatigue limit in a short time.

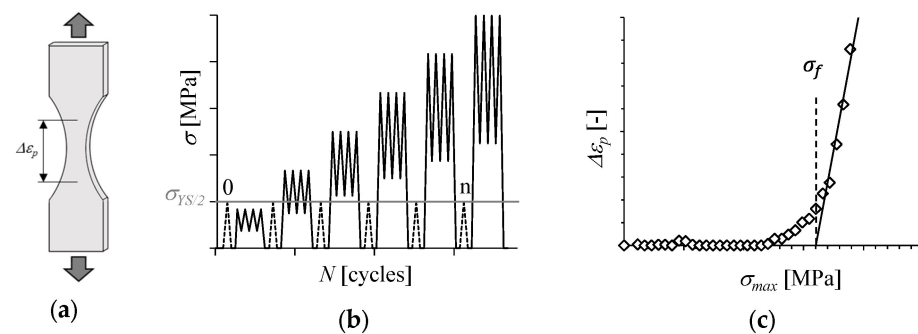


Figure 2. Schematic representation for (a) fatigue specimen geometry; (b) successive fatigue blocks with increasing stress amplitude and strain measurements to determine the fatigue damage; (c) inelastic strain range (white rhombus) versus maximum stress to determine the fatigue limit through the fitting line.

Staircase and rapid tests were performed at room temperature using a stress-controlled servo-hydraulic testing machine MTS 322 Test Frame. The loading frequency was set at 30 Hz with a sinusoidal wave. Thinner specimens were tested at a stress ratio ($R = \sigma_{min}/\sigma_{max}$) of 0.1 to prevent buckling issues, while thicker specimens were tested at $R = -1$ to decrease the testing loads. The results obtained from tests at $R = 0.1$ were converted to -1 using the Gerber relation to allow for comparison purposes.

Fatigue resistance was evaluated for two different edge conditions: *polished* and *sheared*. The specimens with polished edges were machined perpendicularly to the rolling direction using an electro-discharging machine (EDM). Only the edges were ground and polished up to a $R_a < 0.2$ mm, while the surface of the material was left in the as-rolled condition. The specimens with sheared edges were also machined perpendicularly to the rolling direction. For thin materials below 3 mm, a rigid trimming tool was used to obtain the dog-bone specimen geometry shown in Figure 3a, while for thicker ones, a rigid punching tool with a 10 mm punch diameter was used to obtain the open-hole specimen geometry depicted in Figure 3b. This strategy was used owing to the elevated loads required to shear thick high-strength steels. The stress concentration factors (K_t) were calculated through numerical modelling, and their values are presented in Figure 3. Both geometries in conventional tensile and in the normal location of failure onset exhibit a stress triaxiality of 0.33 at maximum force, which is in agreement with the results reported by several authors [39,40]. The shearing clearances specified in Table 3 are commonly used in chassis parts to avoid burrs and excessive deformation of the edge [21,41].

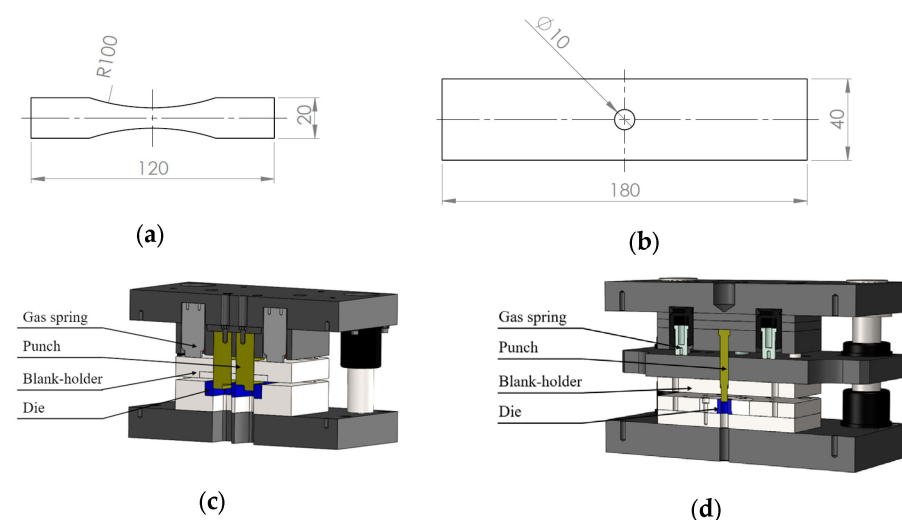


Figure 3. Fatigue specimens with (a) trimmed edges ($K_t = 1.03$) and (b) punched holes ($K_t = 2.42$). Rigid tools designed to (c) trim and (d) punch specimens. The dimensions are expressed in mm.

2.3. Fracture Toughness Tests

The essential work of fracture (EWF) methodology was employed to measure fracture toughness. This method has been extensively used to describe the ductile fracture of thin and thick high-strength steels [42,43]. Such ductile fracture results from combining two parameters that belong to the inner fracture process zone (FPZ) and the outer plastic region during ductile fracture. The work developed in the FPZ is named the essential work of fracture (W_e), which describes the required energy to create new fracture surfaces at the front of the crack tip, and then, it is proportional to the fractured area. On the other hand, the work dissipated in the outer plastic region is called the non-essential plastic work (W_p) and strongly depends on the deformed volume surrounding the fracture plane. Thus, the total work of ductile fracture can be expressed as:

$$W_f = W_e + W_p = w_e l_0 t_0 + \beta w_p l_0^2 t_0 \quad (2)$$

where w_e is the specific essential work of fracture per unit of area, l_0 is the ligament length, t_0 is the specimen thickness, w_p is the specific non-essential plastic work per unit of volume, and β is a shape factor that depends on the shape of the plastic region. Equation (2) can be normalised by the cross-section area resulting in the following:

$$\frac{W_f}{l_0 t_0} = w_f = w_e + \beta w_p l_0 \quad (3)$$

By plotting a series of w_f for different ligament lengths (l_0), a linear fitting can be used to obtain w_e as the intercept in the y -axis and the βw_p as the slope, as shown in Figure 4. The w_f values are experimentally obtained by measuring the area under the load-displacement curves (W_f) for each l_0 and dividing it by the cross-section $l_0 t_0$. As previously described, the nature of w_e makes it suitable to describe the crack propagation resistance of ductile steels, and conceptually, it is equivalent to the J -integral [44].

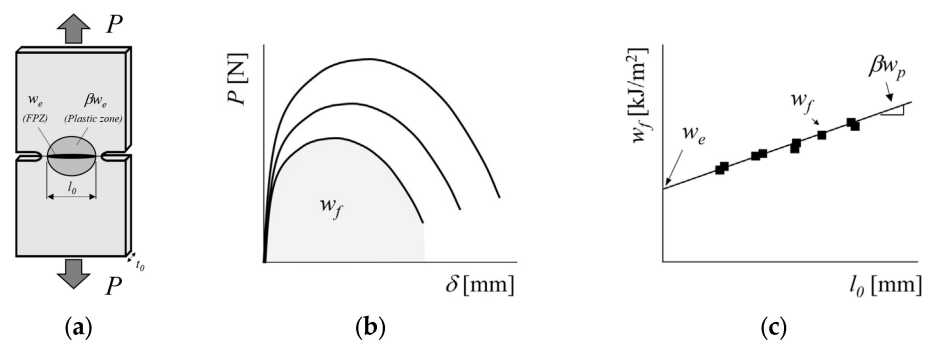


Figure 4. Schematic representation for (a) DENT specimen geometry; (b) load (P)-displacement (δ) curves of each ligament length; (c) specific work of fracture (black square) versus ligament length to determine the specific essential work of fracture and non-essential plastic work through the fitting line.

The testing procedure described in CWA 17793 [45] was followed to conduct the tests. Double Edge Notched Tensile (DENT) specimens, as shown in Figure 5a, were utilised to test thin materials ($t = 1.5$ – 2 mm). The specimens were machined transverse to the rolling direction using electrical discharge machining (EDM), and a pre-crack of at least 0.5 mm was propagated in the root of the machined notches using a resonance fatigue testing machine at $R = 0.1$. The pre-cracked specimens were then loaded monotonically until fracture in a universal testing machine at a crosshead speed of 1 mm/min. A video extensometer with an L_0 of 50 mm directly measured the displacement on the specimen. The ligament lengths of the specimens ranged from 6 to 16 mm, and at least 3 specimens were tested up to fracture for each ligament length.

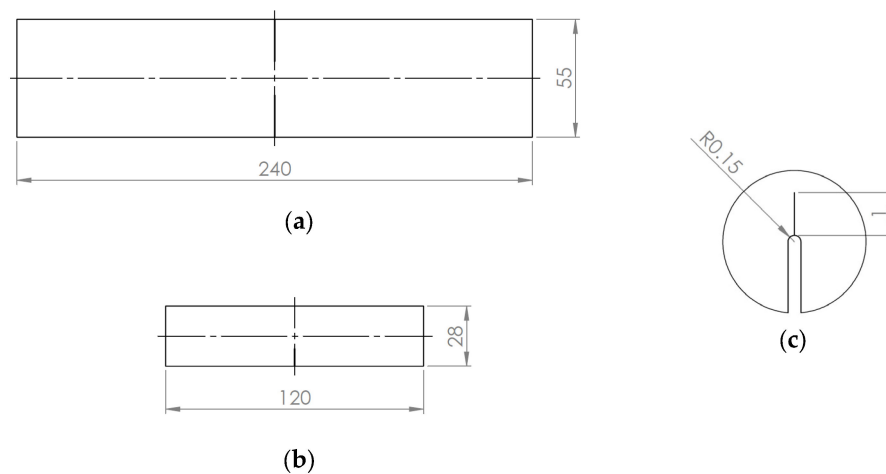


Figure 5. Fracture toughness specimen geometries: (a) DENT and (b) SENB and (c) detail of the EDM notches with fatigue pre-cracks. The dimensions are expressed in mm.

For materials thicker than 2 mm, single edge notch bending (SENB) specimens were machined transverse to the rolling direction, as shown in Figure 5b. It is recommended to use the SENB geometry for thick materials to avoid asymmetrical pre-cracks that may lead to increased scatter and reduce the required maximum load to break the specimens [46]. The specimens were fatigue pre-cracked at $R = 0.1$, following the guidelines of ASTM E1820 to avoid plasticity at the crack tip. A universal testing machine was used to test the specimens with a 3-point bending rig. The tests were conducted at a constant crosshead displacement of 1 mm/min. The crosshead displacement and the load were recorded during the test.

3. Results and Discussion

3.1. Influence of Sheared Edge Defects on Fatigue Resistance

Figure 6 depicts edge surface examples obtained using 3D profilometry for the S500MC and S700MC. The edges display the characteristic zones from the shearing process: the smooth or burnish zone and fracture zone [47]. Despite the nearly identical shearing clearance, the shape of the punched edges differs significantly. In the case of S500MC, approximately one-third of the edge thickness belongs to the fracture zone, while the remaining two-thirds belong to the smooth zone. Conversely, for S700MC, the smooth zone only accounts for one-third of the punched edge, with the majority of the edge belonging to the fracture zone.

The observed differences in the proportions of sheared zones are closely linked to the material properties, including strength, fracture resistance, and thickness. The characteristics of the edge can have a significant impact on the fatigue resistance of the material due to the presence of irregularities such as microcracks or small defects within the fracture zone, the transition zone between the smooth and fracture zones, or the burr. These irregularities act as stress raisers, inducing crack initiation [48]. Figure 7 illustrates a representative fractography observed in high-strength materials with a σ_{YS} above 500 MPa. The fractography provides compelling evidence that edge irregularities serve as fatigue crack initiation sites. Notably, the fatigue origins are primarily situated at the fracture zone of the cut edge, and the resulting cracks propagate through the material in a transgranular manner. Conversely, the MS300 shows ductile fracture behaviour, which can be directly attributed to the significant plasticity induced within the material, as stated in Section 3.2. In this particular case, no conclusive evidence suggests that defects play a role in triggering crack initiation. Meanwhile, the roughness or defects on the as-rolled sheet surface govern the fatigue resistance of the edge-polished specimens. The cracks in both cases initiate and propagate in mode I, perpendicular to the loading direction.

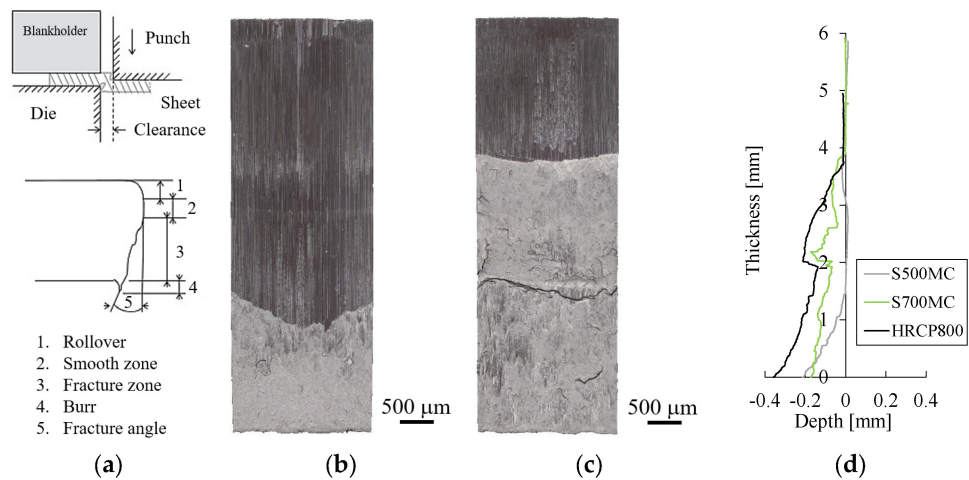


Figure 6. (a) Schematic of the shearing process and edge characteristics. Punched edge surface examples acquired through an optical profilometer for (b) S500MC and (c) S700MC. (d) Edge profiles obtained by 3D profilometry for the S500MC, S700MC, and HRC P800.

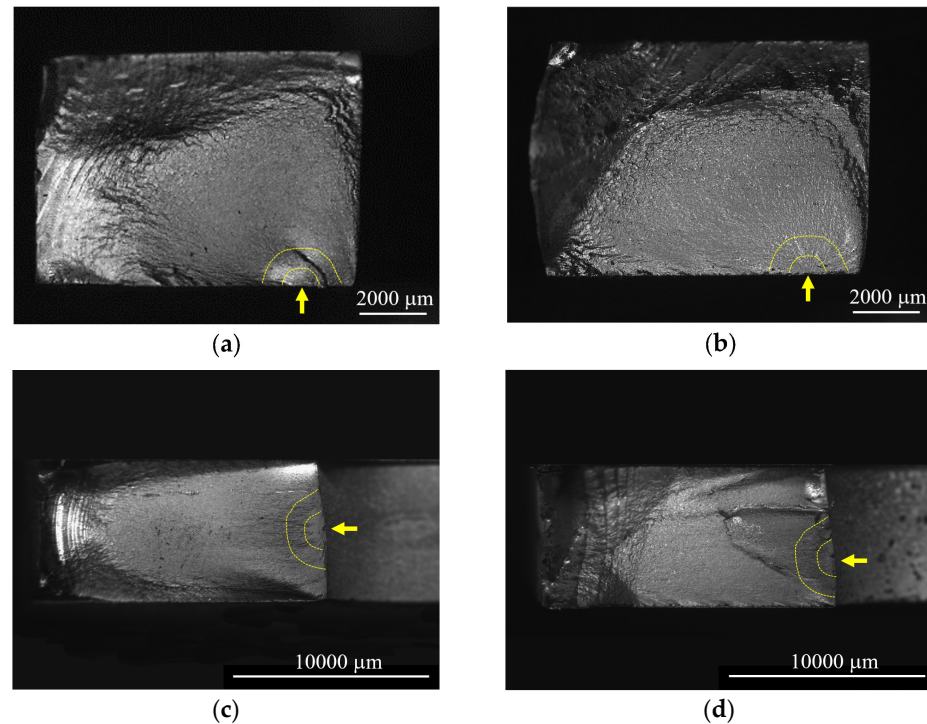


Figure 7. Representative fatigue crack initiation and propagation for polished specimens of (a) WL750 and (b) WL1150 and punched specimens of (c) WL 750 and (d) WL1150. Yellow arrows indicate the crack initiation sites in all the specimens.

Table 3 presents the fatigue resistance of various materials under polished conditions, with the martensitic materials WL1150 and WL980 exhibiting the highest fatigue resistance, while the ferritic–pearlitic MS300 displays the lowest. This trend is consistent with the widely accepted notion that σ_f increases with increasing tensile strength (σ_{UTS}), as illustrated in Figure 8a [49]. However, it is also acknowledged that increasing σ_{UTS} decreases the tolerance against small defects under fatigue loading [48,50]. This fatigue sensitivity can be quantified by calculating the fatigue strength reduction factor (k_f), which takes into account the fatigue resistance of the sheared and polished edge at 2×10^6 cycles:

$$k_f = \frac{\sigma_{f-Sheared}}{\sigma_{f-Polished}} \quad (4)$$

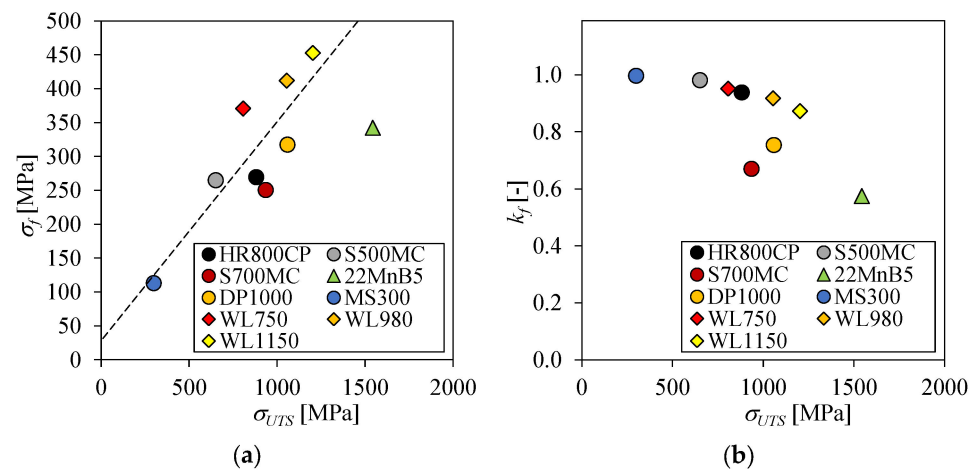


Figure 8. (a) Fatigue resistance of polished specimens (σ_f) against tensile strength (σ_{UTS}) for the investigated steels. The dashed line is a visual guide to show the increasing trend of both properties. (b) Fatigue strength reduction factor (k_f) as a function of the tensile strength (σ_{UTS}).

Values of k_f close to 1 indicate low or no fatigue sensitivity to pre-existing defects. In contrast, lower k_f values correspond to greater fatigue sensitivity to defects and, consequently, lower fatigue limit of defect-containing specimens. Figure 8b illustrates the plot of k_f against σ_{UTS} for the studied materials, highlighting that σ_{UTS} is not the most effective indicator of fatigue sensitivity. In this case, 2 materials, S700MC and HR800CP, with similar σ_{UTS} values, exhibit different k_f values. This phenomenon can be attributed to the fact that the fatigue resistance of sheared edge specimens is primarily determined by the material's ability to resist the propagation of edge defects. Therefore, as described in the subsequent paragraphs, the resistance to crack propagation, i.e., fracture toughness, should also be considered.

Table 3. Fatigue and fracture toughness results for the nine investigated materials: fatigue limit (σ_f) at $R = -1$ (results from tests at R of 0.1 are converted using the Gerber relation) for each edge condition, clearance (Cl), fatigue strength reduction factor (k_f), and fracture toughness (w_e).

Steel Grade	Edge Condition	σ_f [MPa]	k_f	w_e [kJ/m ²]
MS300	Polished	113 ± 5	1.00	289 ± 12
	Trimmed, Cl = 10%	113 ± 6		
S500MC	Polished	265 ± 10	0.98	367 ± 67
	Punched, Cl = 6%	260 ± 24		
WL750	Polished	371 ± 14	0.95	344 ± 49
	Punched, Cl = 10%	353 ± 11		
HR800CP	Polished	270 ± 23	0.94	302 ± 60
	Punched, Cl = 10%	253 ± 19		
S700MC	Polished	251 ± 22	0.67	191 ± 15
	Punched, Cl = 6%	168 ± 12		
WL980	Polished	412 ± 16	0.92	241 ± 56
	Punched, Cl = 10%	378 ± 2		
DP1000	Polished	317 ± 3	0.75	203 ± 17
	Trimmed, Cl = 6%	239 ± 40		
WL1150	Polished	453 ± 22	0.87	192 ± 22
	Trimmed, Cl = 6%	395 ± 12		
22MnB5	Polished	343 ± 38	0.57	159 ± 11
	Trimmed, Cl = 6%	197 ± 23		

3.2. Damage-Tolerant Fatigue Design Approach

The behaviour of materials containing defects can be addressed by employing a defect-tolerant fatigue design approach, which assumes that defects can be treated as effective cracks that propagate once a certain threshold is exceeded. This approach is commonly

rationalised within the framework of linear elastic fracture mechanics (LEFM), where a pre-existent defect (a) propagates under cyclic loading ($\Delta\sigma$) once the threshold stress intensity factor range (ΔK_{th}) is attained:

$$\Delta K_{th} = Y\Delta\sigma\sqrt{\pi a} \quad (5)$$

where Y is a dimensionless factor related to the geometry of the crack. However, the application of LEFM is limited to the cyclic fracture resistance of a material when the small-scale yielding condition is dominant. This condition stipulates that the plastic zone at the crack tip (r_c) must be smaller than the defect size. When a/r_c is greater than 10 (or $r_c/a < 0.1$), the plastic zone is considered to be small, and the small-scale yielding condition is valid [51]. The size of the cyclic plastic zone was determined by the Dugdale approach using the data from Tables 2 and 3 [52].

$$\frac{r_c}{a} = \left(\sec \frac{\pi\sigma_f}{2\sigma_{YS}} - 1 \right) \quad (6)$$

Based on the calculated r_c/a values, the use of LEFM is limited to 22MnB5 and S700MC ($r_c/a < 0.1$), as the plastic zone of the remaining materials is too large to satisfy the small-scale yielding conditions (r_c/a between 0.12 and 0.29), with MS300 being clearly outside this regime (r_c/a of 0.46). In such cases, the shear edge defects of these materials can be treated as mechanically small cracks as their size is comparable to the plastic zone [53], precluding the application of LEFM to describe their propagation. Instead, the propagation of such defects can be described using the \sqrt{area} parameter proposed by Murakami et al. [54]. Based on such an empirical approach—and considering that strength may be estimated from the Vickers hardness (HV)—some equations were proposed to estimate the length of the equivalent critical crack ($\sqrt{area}_{critical}$) from HV, such as the one presented below [55]:

$$\sqrt{area}_{critical} = 0.51 \left(1 + \frac{120}{HV} \right)^6 \quad (7)$$

The equation can be employed to assess if the defects at the sheared edge for the studied material are sufficiently large to propagate under fatigue. Specifically, the $\sqrt{area}_{critical}$ value was calculated for each material, with the σ_{UTS} converted to HV according to ISO 18265. The defects at the sheared edge were quantified through the parameter R_v , defined as the deepest valley from the surface profile, obtained via profilometry measurements at both the fracture and smooth zones. This parameter was established as an effective means of characterising the critical defect that initiates fatigue in press-hardened steels [34]. R_v ranges from 30 (for the S500MC) to 60 μm (for the HR800CP). Figure 9 depicts the estimated values of $\sqrt{area}_{critical}$. For the low strength MS300 (with σ_{UTS} of 300 MPa), the calculated $\sqrt{area}_{critical}$ is 70 μm , which is greater than the measured shear edge defects ($R_v = 49 \pm 15 \mu\text{m}$). This suggests that edge cracks in MS300 will not propagate, and therefore, that the fatigue resistance of sheared and polished specimens should be similar. This is consistent with the results presented in Table 3, where the fatigue resistance of the polished and trimmed conditions is identical. On the other hand, for steels with σ_{UTS} above 500 MPa, the calculated $\sqrt{area}_{critical}$ is lower than 10 μm , which is lower than the sheared edge defects. This means that such defects will propagate under fatigue, resulting in a lower fatigue limit for specimens with sheared edges. This agrees with the findings shown in Table 3. However, Figure 9 indicates that there is no clear correlation between $\sqrt{area}_{critical}$ and σ_f for the sheared specimens, which is illustrated by instances where the value of $\sqrt{area}_{critical}$ is similar but the fatigue resistance is different. Hence, it is not recommended to rely solely on $\sqrt{area}_{critical}$ as a reliable predictor of the fatigue resistance of sheared specimens.

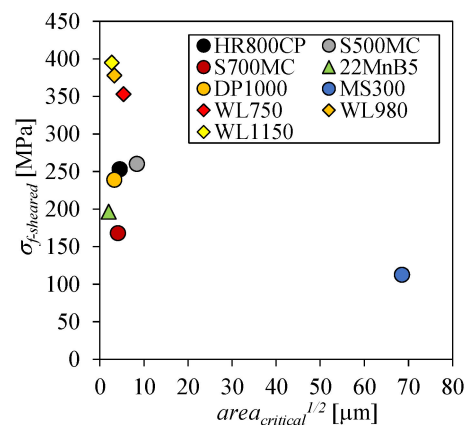


Figure 9. Fatigue resistance of sheared specimens ($\sigma_{f-sheared}$) against estimated $\sqrt{area_{critical}}$ for the investigated steels.

The new generation of high-strength steels, as the ones analysed here, have optimised microstructures to reach high toughness together with high strength, so the effect of both properties on fatigue resistance should be considered. Tough materials, evidenced as steels with $w_e > 250$ kJ/m² in Table 3, exhibit high resistance to monotonic crack propagation, which could enhance fatigue performance. This contribution may be particularly significant in the case of sheared specimens, where defects are already present and most of the fatigue life is related to the cyclic propagation of these defects.

3.3. Relationship between Fracture Toughness and Fatigue Notch Sensitivity

The fatigue propagation of mechanically small cracks can be described by using an elastic–plastic fracture mechanics approach, as proposed by Dowling and Begley [56] through the cyclic *J-integral* (ΔJ) [57,58]. This method has been successfully applied to describe the cyclic driving force in fatigue crack propagation of surface cracks in welds, which may be similar to edge defects [59]. As ΔJ is an extension of the monotonic *J-integral* introduced by Rice [60], w_e (equivalent to J_{Ic}) can be used to understand fatigue crack propagation. Figure 10 illustrates how w_e can effectively rank the fatigue sensitivity, k_f . Both parameters show a strong positive correlation according to the calculated Pearson correlation coefficient (r) value of 0.83. Materials with low toughness (low values of w_e) are more sensitive to defects (low values of k_f), because of the scarce energy available to resist crack propagation of pre-existing defects. This indicates that low-toughness materials have high fatigue notch sensitivity and low damage tolerance. Conversely, tough materials with high values of w_e exhibit low sensitivity to surface defects (k_f close to 1), as the material offers high resistance to crack propagation. Therefore, the fatigue limit of polished and sheared specimens will be similar, indicating that high-toughness materials ($w_e > 250$ kJ/m²) have high damage tolerance and low fatigue notch sensitivity. This is mainly due to the higher fracture energy required to propagate the already nucleated defects. Frómeta et al., also reported this energy level of 250 kJ/m² as an indicator of high edge cracking resistance [14] and crashworthiness [43] in advanced high strength steels.

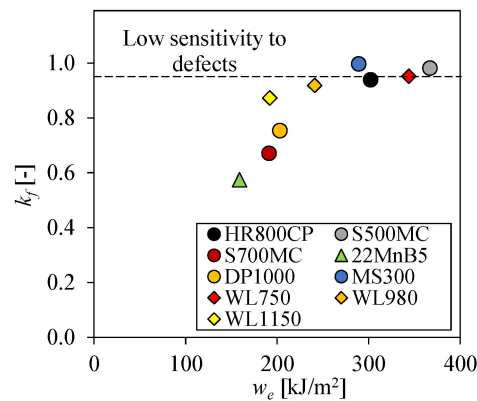


Figure 10. Fatigue strength reduction factor (k_f) as a function of fracture toughness (w_e).

3.4. Implications on the Design of Fatigue-Relevant Parts

To select materials with high fatigue performance, it is important to consider both the fatigue limit and the fatigue notch sensitivity. Fracture toughness is a property that can represent the fatigue notch sensitivity, and thus, plotting the fatigue resistance of materials in the polished condition (σ_f) against their fracture toughness (w_e) provide valuable information for material selection (Figure 11). It is important to note that a moderate negative correlation ($r = -0.31$) has been observed, indicating a decrease in fatigue strength as fracture toughness increases. This tendency is similar with the observed inverse relationship between fracture toughness and yield strength [61]. However, it is worth mentioning that the enhanced microstructures of new high-strength steels exhibit not only high yield strength but also higher fracture toughness values [14]. These advancements challenge the traditional understanding of the relationship between fracture toughness and yield strength usually related to fatigue strength [62]. Then, the ideal materials for fatigue dimensioning parts would be located in the upper right corner of the plot. The behaviour of the studied materials in this fatigue-toughness plot can be described as follows:

- DP1000 and S700MC have high fatigue limits but low toughness (<250 kJ/m²), resulting in low damage tolerance or high fatigue notch sensitivity;
- The 22MnB5 steel shows excellent formability in hot conditions and superior fatigue resistance, making it a good candidate for lightweighting. However, its high sensitivity to defects (low fracture toughness) indicates that special attention must be paid during component designing and manufacturing. Similar behaviour is found for WL1150;
- WL750, WL980, HR800CP, and S500MC exhibit high fatigue limits and low fatigue notch sensitivity, which postulate them as good candidates for chassis lightweighting strategies. In general, warm-formed steels (WL780, WL980, WL1150) show a good combination of high fatigue limit and fracture toughness. This optimised performance, together with the high formability of these steel grades at the manufacturing temperatures, even for thick sheets, poses them as excellent candidates for truck chassis parts.

4. Conclusions

This study demonstrates that the fatigue resistance of the material, measured in polished specimens, and the fracture toughness, measured in the frame of elastic-plastic fracture mechanics, may be used in tandem to select high-strength material for lightweighting fatigue-dimensioning parts. The experimental results lead to the following conclusions:

- The fatigue resistance of both edge-polished and sheared specimens can be measured in 3–4 h using the *stiffness method*;
- The influence of the sheared edge quality on the fatigue resistance can be quantified by a fatigue strength reduction factor (k_f). Such factor accounts for the fatigue notch sensitivity; low values of k_f around 0.5 mean high fatigue notch sensitivity or low fatigue damage tolerance, meanwhile values of k_f close to 1 indicate low fatigue notch sensitivity or high fatigue damage tolerance;

- The k_f factor correlates well with the fracture toughness, determined by the essential work of fracture methodology, reporting a correlation coefficient (r) value of 0.83. Accordingly, tough materials such as the WL750 ($w_e = 344 \pm 49 \text{ kJ/m}^2$) show low fatigue notch sensitivity, while low-toughness materials such as the 22MnB5 ($w_e = 159 \pm 11 \text{ kJ/m}^2$) have high fatigue notch sensitivity. A w_e of 250 kJ/m^2 can be defined as a threshold for a low fatigue sensitivity to surface defects, for the studied materials;
- Despite the moderate correlation between fatigue and fracture toughness parameters ($r = -0.31$), the plot permits ranking of the material candidates to be used for a lightweight fatigue design of chassis parts. Following such results, the warm-formed steels stand out as one of the best candidates, showing good fatigue resistance above the reference material and fracture toughness higher than the w_e threshold.

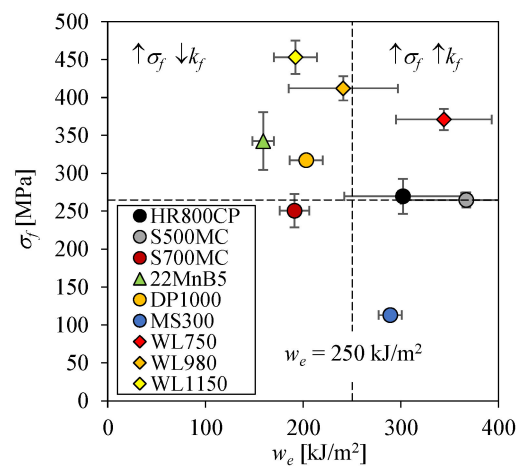


Figure 11. Fatigue resistance of polished specimens (σ_f) against fracture toughness (w_e) for the investigated steels. The dashed lines represent the reference fatigue resistance and the fracture toughness threshold.

Author Contributions: Conceptualisation, S.P. and D.C.; writing—original draft preparation S.P.; writing—review and editing, S.P., D.C., D.F. A.M. and H.S.; mechanical tests, S.P., D.F. and H.S.; data analysis, S.P. and D.F.; supervision D.C. and A.M. All authors have read and agreed to the published version of the manuscript.

Funding: This research received no external funding.

Data Availability Statement: Not applicable.

Acknowledgments: A.M. acknowledges the Agència de Gestió d'Ajuts Universitaris i de Recerca (AGAUR) del Departament de Recerca i Universitats de la Generalitat de Catalunya for recognising the Microstructural Design and Advanced Manufacturing of Materials Group as a consolidated research group number 2021 SGR 01053.

Conflicts of Interest: The authors declare no conflict of interest.

References

1. Decker, M. Vibration fatigue analysis using response spectra. *Int. J. Fatigue* **2021**, *148*, 106192. [[CrossRef](#)]
2. Bellec, E.; Facchinetti, M.; Doudard, C.; Calloch, S.; Moyne, S.; Silvestri, M. Modelling and identification of fatigue load spectra: Application in the automotive industry. *Int. J. Fatigue* **2021**, *149*, 106222. [[CrossRef](#)]
3. Sonsino, C. Consideration of salt-corrosion fatigue for lightweight design and proof of aluminium safety components in vehicle applications. *Int. J. Fatigue* **2021**, *154*, 106406. [[CrossRef](#)]
4. Sonsino, C.; Breitenberger, M.; Krause, I.; Pötter, K.; Schröder, S.; Jürgens, K. Required Fatigue Strength (RFS) for evaluating of spectrum loaded components by the example of cast-aluminium passenger car wheels. *Int. J. Fatigue* **2020**, *145*, 105975. [[CrossRef](#)]
5. Stellmach, S.; Braun, L.; Wächter, M.; Esderts, A.; Diekhaus, S. On load assumptions for self-propelled forage harvesters. *Int. J. Fatigue* **2021**, *147*, 106114. [[CrossRef](#)]
6. De Almeida, D.T.; Bianchi, K.E.; de Souza, J.H.C.; de Lima, M.S.F.; Clarke, T.G.R.; da Silva, F.P.; Mohrbacher, H. Fatigue Performance of Laser Welds in Heavy-Gage Press Hardening Steels. *Metals* **2022**, *12*, 580. [[CrossRef](#)]

7. Cecchel, S. Materials and Technologies for Lightweighting of Structural Parts for Automotive Applications: A Review. *SAE Int. J. Mater. Manuf.* **2020**, *14*, 81–98. [[CrossRef](#)]
8. Zhang, W.; Xu, J. Advanced lightweight materials for Automobiles: A review. *Mater. Des.* **2022**, *221*, 110994. [[CrossRef](#)]
9. Hattalli, V.L.; Srivatsa, S.R. Sheet Metal Forming Processes—Recent Technological Advances. *Mater. Today Proc.* **2018**, *5*, 2564–2574. [[CrossRef](#)]
10. Diaz-Infante, D.; Narayanan, A.; Groseclose, A.; Altan, T. *FE Simulations of Piercing and Trimming of AL and AHSS Alloys*; Springer: Berlin/Heidelberg, Germany, 2021; pp. 2925–2938. [[CrossRef](#)]
11. Nothhaft, K.; Suh, J.; Golle, M.; Picas, I.; Casellas, D.; Volk, W. Shear cutting of press hardened steel: Influence of punch chamfer on process forces, tool stresses and sheared edge qualities. *Prod. Eng.* **2012**, *6*, 413–420. [[CrossRef](#)]
12. Senn, S.; Liewald, M. Experimental investigation of piercing of high-strength steels within a critical range of slant angle. *J. Physics Conf. Ser.* **2017**, *896*, 12099. [[CrossRef](#)]
13. Sandin, O.; Hammarberg, S.; Parareda, S.; Frómeta, D.; Casellas, D.; Jonsén, P. Prediction of sheared edge characteristics of advanced high strength steel. *IOP Conf. Ser. Mater. Sci. Eng.* **2022**, *1238*, 012034. [[CrossRef](#)]
14. Frómeta, D.; Lara, A.; Grifé, L.; Dieudonné, T.; Dietsch, P.; Rehl, J.; Suppan, C.; Casellas, D.; Calvo, J. Fracture Resistance of Advanced High-Strength Steel Sheets for Automotive Applications. *Met. Mater. Trans. A* **2021**, *52*, 840–856. [[CrossRef](#)]
15. Casellas, D.; Lara, A.; Frómeta, D.; Gutiérrez, D.; Molas, S.; Pérez, L.; Rehl, J.; Suppan, C. Fracture Toughness to Understand Stretch-Flangeability and Edge Cracking Resistance in AHSS. *Met. Mater. Trans. A* **2016**, *48*, 86–94. [[CrossRef](#)]
16. Lipiäinen, K.; Kaijalainen, A.; Ahola, A.; Björk, T. Fatigue strength assessment of cut edges considering material strength and cutting quality. *Int. J. Fatigue* **2021**, *149*, 106263. [[CrossRef](#)]
17. Thomas, D.J. A Review of Fatigue Failure Properties from Edge Defects. *J. Fail. Anal. Prev.* **2017**, *17*, 802–811. [[CrossRef](#)]
18. Meurling, F.; Melander, A.; Linder, J.; Larsson, M. The influence of mechanical and laser cutting on the fatigue strengths of carbon and stainless sheet steels. *Scand. J. Met.* **2001**, *30*, 309–319. [[CrossRef](#)]
19. Thum, M.; Basavarajappa, V.; Haefele, P. Influence of edge cutting process on fatigue behaviour of spectrum loaded aluminum sheets. *Int. J. Fatigue* **2021**, *150*, 106330. [[CrossRef](#)]
20. Zhang, K.; Hamada, S.; Yokoi, T.; Noguchi, H. Significant reduction of fatigue crack non-propagation limit caused by damage accumulation mode fatigue crack propagation in a precipitation-hardened punched steel plate. *Mater. Sci. Eng. A* **2023**, *871*, 144871. [[CrossRef](#)]
21. Stahl, J.; Pätzold, I.; Golle, R.; Sunderkötter, C.; Sieurin, H.; Volk, W. Effect of One- and Two-Stage Shear Cutting on the Fatigue Strength of Truck Frame Parts. *J. Manuf. Mater. Process.* **2020**, *4*, 52. [[CrossRef](#)]
22. Remes, H.; Korhonen, E.; Lehto, P.; Romanoff, J.; Niemelä, A.; Hiltunen, P.; Kontkanen, T. Influence of surface integrity on the fatigue strength of high-strength steels. *J. Constr. Steel Res.* **2013**, *89*, 21–29. [[CrossRef](#)]
23. Lillemäe-Avi, I.; Liinalampi, S.; Lehtimäki, E.; Remes, H.; Lehto, P.; Romanoff, J.; Ehlers, S.; Niemelä, A. Fatigue strength of high-strength steel after shipyard production process of plasma cutting, grinding, and sandblasting. *Weld. World* **2018**, *62*, 1273–1284. [[CrossRef](#)]
24. Jin, Z.; Mallick, P.K. Enhancement of Fatigue Life of Self-Piercing Riveted Joints by Coining. *Manufacturing* **2002**, *2002*, 417–429. [[CrossRef](#)]
25. Diekhoff, P.; Hensel, J.; Nitschke-Pagel, T.; Dilger, K. Investigation on fatigue strength of cut edges produced by various cutting methods for high-strength steels. *Weld. World* **2020**, *64*, 545–561. [[CrossRef](#)]
26. Lipiäinen, K.; Ahola, A.; Skriko, T.; Björk, T. Fatigue strength characterization of high and ultra-high-strength steel cut edges. *Eng. Struct.* **2020**, *228*, 111544. [[CrossRef](#)]
27. Stenberg, T.; Lindgren, E.; Barsoum, Z.; Barmicho, I. Fatigue assessment of cut edges in high strength steel—Influence of surface quality. *Mater. Werkst.* **2017**, *48*, 556–569. [[CrossRef](#)]
28. Zhu, S.-P.; Ye, W.-L.; Correia, J.A.; Jesus, A.M.; Wang, Q. Stress gradient effect in metal fatigue: Review and solutions. *Theor. Appl. Fract. Mech.* **2022**, *121*, 103513. [[CrossRef](#)]
29. Liu, M.; Miranda, A.C.D.O.; Antunes, M.A.; Meggiolaro, M.A.; de Castro, J.T.P. Plastic stress concentration effects in fatigue strength. *Int. J. Fatigue* **2023**, *168*, 107394. [[CrossRef](#)]
30. Pirinu, A.; Panella, F.W. A new approach for rapid fatigue limit assessment for C45 steel based on contrast damage parameters. *Mech. Res. Commun.* **2023**, *127*, 104039. [[CrossRef](#)]
31. Foti, P.; Santonocito, D.; Ferro, P.; Risitano, G.; Berto, F. Determination of Fatigue Limit by Static Thermographic Method and Classic Thermographic Method on Notched Specimens. *Procedia Struct. Integr.* **2020**, *26*, 166–174. [[CrossRef](#)]
32. De Finis, R.; Palumbo, D.; Pirinu, A.; Saponaro, A.; Panella, F.W.; Nobile, R.; Galietti, U. Fatigue behaviour assessment of C45 steel by means of energy-based methods. *IOP Conf. Ser. Mater. Sci. Eng.* **2021**, *1038*, 012015. [[CrossRef](#)]
33. Giudice, F.; La Rosa, G.; Savio, F.L.; Clienti, C. Comparison between thermal energy and acoustic emission for the fatigue behavior of steels. *Procedia Struct. Integr.* **2019**, *18*, 886–890. [[CrossRef](#)]
34. Parareda, S.; Casellas, D.; Frómeta, D.; Martínez, M.; Lara, A.; Barrero, A.; Pujante, J. Fatigue resistance of press hardened 22MnB5 steels. *Int. J. Fatigue* **2019**, *130*, 105262. [[CrossRef](#)]
35. Mughrabi, H. On ‘multi-stage’ fatigue life diagrams and the relevant life-controlling mechanisms in ultrahigh-cycle fatigue. *Fatigue Fract. Eng. Mater. Struct.* **2002**, *25*, 755–764. [[CrossRef](#)]

36. Bellec, E.; Doudard, C.; Facchinetti, M.; Calloch, S.; Moyne, S. Loading Classification Proposal for Fatigue Design of Automotive Chassis-Parts: A Relevant Process for Variable Amplitude and Multi-Input Load Cases. *Int. J. Fatigue* **2022**, *166*, 107284. [[CrossRef](#)]
37. Dixon, W.J.; Mood, A.M. A Method for Obtaining and Analyzing Sensitivity Data. *J. Am. Stat. Assoc.* **1948**, *43*, 109–126. [[CrossRef](#)]
38. Parareda, S.; Casellas, D.; Lara, A.; Mateo, A. Fatigue resistance evaluation of high Mn-TWIP steel through damage mechanics: A new method based on stiffness evolution. *Int. J. Fatigue* **2021**, *156*, 106643. [[CrossRef](#)]
39. Bao, Y.; Wierzbicki, T. On fracture locus in the equivalent strain and stress triaxiality space. *Int. J. Mech. Sci.* **2004**, *46*, 81–98. [[CrossRef](#)]
40. Sandin, O.; Jonsén, P.; Frómeta, D.; Casellas, D. Stating Failure Modelling Limitations of High Strength Sheets: Implications to Sheet Metal Forming. *Materials* **2021**, *14*, 7821. [[CrossRef](#)]
41. Parareda, S.; Lara, A.; Sieurin, H.; D'armas, H.; Casellas, D. Increasing fatigue performance in AHSS thick sheet by surface treatments. *MATEC Web Conf.* **2018**, *165*, 22015. [[CrossRef](#)]
42. Frómeta, D.; Parareda, S.; Lara, A.; Casellas, D.; Pujante, J.; Jonsén, P.; Golling, S.; Sieurin, H.; Oldenburg, M. Fracture toughness evaluation of thick press hardened 22MnB5 sheets for high crash performance applications in trucks. In Proceedings of the 7th International Conference on Hot Sheet Metal Forming of High Performance Steel (CHS2 2019), Luleå, Sweden, 2–5 June 2019.
43. Frómeta, D.; Lara, A.; Molas, S.; Casellas, D.; Rehrl, J.; Suppan, C.; Larour, P.; Calvo, J. On the correlation between fracture toughness and crash resistance of advanced high strength steels. *Eng. Fract. Mech.* **2018**, *205*, 319–332. [[CrossRef](#)]
44. Frómeta, D.; Parareda, S.; Lara, A.; Molas, S.; Casellas, D.; Jonsén, P.; Calvo, J. Identification of fracture toughness parameters to understand the fracture resistance of advanced high strength sheet steels. *Eng. Fract. Mech.* **2020**, *229*, 106949. [[CrossRef](#)]
45. European Committee for Standardization. *Test Method for Determination of the Essential Work of Fracture of Thin Ductile Metallic Sheets*; CEN-CENELE: Brussels, Belgium, 2021.
46. Tarhouni, I.; Frómeta, D.; Casellas, D. Essential work of fracture method for toughness evaluation of thick press hardened 22MnB5 plates. In Proceedings of the 8th International Conference on Hot Sheet Metal Forming of High Performance Steel (CHS2 2022), Wissenschaftliche Scripten, Barcelona, Spain, 30 May–2 June 2022.
47. The Association of German Engineers. *VDI 2906-2: Quality of Cut Faces of (Sheet) Metal Parts after Cutting, Blanking, Trimming or Piercing*; General Introduction, Characteristic Values, Materials: Berlin, Germany, 1994.
48. Lara, A.; Picas, I.; Casellas, D. Effect of the cutting process on the fatigue behaviour of press hardened and high strength dual phase steels. *J. Mater. Process. Technol.* **2013**, *213*, 1908–1919. [[CrossRef](#)]
49. Murakami, Y. Material defects as the basis of fatigue design. *Int. J. Fatigue* **2012**, *41*, 2–10. [[CrossRef](#)]
50. Schönbauer, B.M.; Mayer, H. Effect of small defects on the fatigue strength of martensitic stainless steels. *Int. J. Fatigue* **2019**, *127*, 362–375. [[CrossRef](#)]
51. Davidson, D.; Chan, K.; McClung, R.; Hudak, S. Small Fatigue Cracks. *Compr. Struct. Integr.* **2003**, *4*, 129–164. [[CrossRef](#)]
52. Dugdale, D.S. Yielding of steel sheets containing slits. *J. Mech. Phys. Solids* **1960**, *8*, 100–104. [[CrossRef](#)]
53. Tanaka, K. Fatigue Crack Propagation. *Compr. Struct. Integr.* **2003**, *4*, 95–127. [[CrossRef](#)]
54. Yukitaka, M.; Masahiro, E. Quantitative evaluation of fatigue strength of metals containing various small defects or cracks. *Eng. Fract. Mech.* **1983**, *17*, 1–15. [[CrossRef](#)]
55. Yang, Z.; Zhang, J.; Li, S.; Li, G.; Wang, Q.; Hui, W.; Weng, Y. On the critical inclusion size of high strength steels under ultra-high cycle fatigue. *Mater. Sci. Eng. A* **2006**, *427*, 167–174. [[CrossRef](#)]
56. Dowling, N.; Begley, J. Fatigue Crack Growth During Gross Plasticity and the J-Integral. In *Mechanics of Crack Growth*; American Society for Testing and Materials: West Conshohocken, PA, USA, 1976; pp. 82–103. [[CrossRef](#)]
57. Zerbst, U.; Madia, M.; Vormwald, M.; Beier, H. Fatigue strength and fracture mechanics—A general perspective. *Eng. Fract. Mech.* **2018**, *198*, 2–23. [[CrossRef](#)]
58. Lesiuk, G.; Szata, M.; Rozumek, D.; Marciniak, Z.; Correia, J.; De Jesus, A. Energy response of S355 and 41Cr4 steel during fatigue crack growth process. *J. Strain Anal. Eng. Des.* **2018**, *53*, 663–675. [[CrossRef](#)]
59. Ngoula, D.T.; Madia, M.; Beier, H.; Vormwald, M.; Zerbst, U. Cyclic J-integral: Numerical and analytical investigations for surface cracks in weldments. *Eng. Fract. Mech.* **2018**, *198*, 24–44. [[CrossRef](#)]
60. Rice, J.R. A Path Independent Integral and the Approximate Analysis of Strain Concentration by Notches and Cracks. *J. Appl. Mech.* **1968**, *35*, 379–386. [[CrossRef](#)]
61. Oh, G. A simplified toughness estimation method based on standard tensile data. *Int. J. Press. Vessel. Pip.* **2022**, *199*, 104733. [[CrossRef](#)]
62. Görzen, D.; Ostermayer, P.; Lehner, P.; Blinn, B.; Eifler, D.; Beck, T. A New Approach to Estimate the Fatigue Limit of Steels Based on Conventional and Cyclic Indentation Testing. *Metals* **2022**, *12*, 1066. [[CrossRef](#)]

Disclaimer/Publisher's Note: The statements, opinions and data contained in all publications are solely those of the individual author(s) and contributor(s) and not of MDPI and/or the editor(s). MDPI and/or the editor(s) disclaim responsibility for any injury to people or property resulting from any ideas, methods, instructions or products referred to in the content.